atmosphere

MDPI

Article

Sensitive Grain-Size Components of Last Glacial Loess on Chinese Loess Plateau and Their Response to East Asian Winter Monsoon

Qiansuo Wang [1,*], Yougui Song [2], Linqiong Duan [1] and Jinchan Li [1]

[1] College of Land and Tourism, Luoyang Normal University, Luoyang 471934, China
[2] State Key Laboratory of Loess and Quaternary Geology, Institute of Earth Environment, Chinese Academy of Sciences, Xi'an 710061, China
* Correspondence: wangqiansuo@lynu.edu.cn or qiansuowang@outlook.com

Abstract: Chinese loess provides the most detailed terrestrial records of paleoclimate changes. We employed the grain-size components of aeolian sediments to reconstruct the history of the East Asian winter monsoon (EAWM) on the Chinese Loess Plateau (CLP). Here, using the grain-size class vs. standard deviation method, we extracted the environmentally sensitive grain-size components of nine last glacial loess sections. The grain-size class vs. standard deviation diagrams showed two major grain-size components (fine and coarse), which varied from section to section. Material resource distances and post-depositional pedogenesis were the main factors affecting environmentally sensitive grain-size components. The coarse grain-size components of the Yulin, Baicaoyuan, Xifeng, and Luochuan sections were influenced by the transportation distance, while we attributed the fine grain-size components of the Weinan, Shaoling, Duanjiapo, and Chaona sections to pedogenesis. At the same time, the Mianchi section's sensitive grain-size component was also coarse, and was affected by the local circulation from the nearby Yellow River terrace. Our comparison of sensitive grain-size components and EAWM revealed that the coarse grain-size components were progressively finer along with the EAWM from the northwest to the southeast on the CLP, and they can be regarded as the most suitable proxy indicator of the EAWM on the CLP.

Keywords: aeolian; grain size; atmospheric circulation; last glacial loess; East Asian winter monsoon

Citation: Wang, Q.; Song, Y.; Duan, L.; Li, J. Sensitive Grain-Size Components of Last Glacial Loess on Chinese Loess Plateau and Their Response to East Asian Winter Monsoon. *Atmosphere* **2023**, *14*, 304. https://doi.org/10.3390/atmos14020304

Academic Editor: Alexey V. Eliseev

Received: 30 November 2022
Revised: 5 January 2023
Accepted: 1 February 2023
Published: 3 February 2023

1. Introduction

The near-continuous Quaternary loess-paleosol sequences and the Neogene red clay deposits on the CLP have provided important information about paleoclimatic and paleoenvironmental changes, with the global climate cooling since the Cenozoic Era and the appearance of inland drought [1–14]. The effects of alternations to loess-paleosol sequences on the CLP are well documented, including the changes brought by the East Asian monsoon (EAM) over the past 2.6 Myr [3,4,7,11–16]. The grain-size proxy exhibits high-quality information on the variability of the EAWM [3,4,7,8,10,14–16]. The grain size and thickness of the last glacial Malan loess (L1) exhibit a clear decreasing trend from northwest to southeast across the CLP [1,17–27], indicating that the EAWM weakened gradually.

Sedimental grain size is a widely used indicator for studying climatic changes and environmental evolution because of its close links to sedimental sources, transport dynamics, and depositional environments [22,28–47]. Previous studies on the grain-size characteristics of modern dust and loess deposits suggested that the grain-size components of aeolian sediments have been employed to reconstruct the history of EAWM, which can provide important information about its provenance and changes in the sedimental environment [26,29,32–34,42,48–51]. A stronger EAWM results in a larger median size and higher coarse-fraction content of dust and loess samples [48,50,52–55]. Grain-size parameters, such as median and mean grain size, size ratio, and coarse-fraction content, are widely

selected for reconstructions of winter monsoon variations [10,24,26,56–58]. Therefore, the grain sizes of loess/paleosol sequences are considered proxies for winter monsoon strength, which can be correlated with Northern and Southern Hemisphere proxy records [26,50].

The grain-size class standard deviation method permits easy identification of the grain-size intervals, with the largest variability along the sedimentary sequences [59]. Additionally, this method has been applied successfully in the research of loess [52,60], lake sediments [61], and marine deposits [53,55,59,62,63]. However, much less is known about the spatial variation characteristics of the environmentally sensitive grain-size components of the last glacial loess. Here, using the grain-size class standard deviation method, we performed an analysis of environmentally sensitive grain-size components from the last glacial loess on the CLP [64–70]. Our objective is to better determine which grain sizes of the loess deposits can be used to delineate variations in EAWM strength.

2. Materials and Methods

In our study, we logged nine last glacial loess sections in the CLP (Table 1), located at Yulin, Baicaoyuan, Xifeng, Luochuan, Chaona, Mianchi, Weinan, Duanjiapo, and Shaoling (Figure 1).

Table 1. Nine last glacial loess sites on the Chinese Loess Plateau.

Sampling	Sections	Samples	Latitude	Longitude	Altitude	L1 Thickness	L1 MGS [1]
Site	Abbreviations		° N	° E	m	m	μm
Yulin	YL	200	38.271	109.792	1197	11.60	62.75
Baicaoyuan	BCY	210	36.218	105.024	1830	13.35	41.33
Xifeng	XF	205	35.783	107.623	1352	11.80	29.41
Luochuan	LC	56	35.752	109.416	1065	8.04	22.37
Chaona	CN	208	35.147	107.224	1464	6.18	21.32
Mianchi	MC	130	34.772	111.777	535	7.12	24.87
Weinan	WN	288	34.415	109.562	787	8.20	18.62
Duanjiapo	DJP	209	34.188	109.233	593	5.00	18.41
Shaoling	SL	91	34.138	108.965	443	6.70	18.15

[1] MGS is mean grain size.

We prepared grain-size samples according to Lu et al.'s pretreatment method [71]. We first pretreated the dry bulk samples weighing 0.3–0.5 g with 30% hydrogen peroxide (H_2O_2) to remove organic matter, and then 10% hydrochloric acid (HCl) to remove calcium carbonate, which ensured that our results reflected the grain-size distribution of the siliciclastic loess fraction. We then suspended the treated samples in deionized water, dispersed with 10 mL 10% $(NaPO_3)_6$ solution, and sonicated and oscillated in an ultrasonic bath for 10 min to completely separate the fine particles. We measured the grain-size distributions using a Mastersizer 2000 which manufactured Malvern, Britain. Replicate analyses indicated that the mean grain size had an analytical error of <3%. We calculated the standard deviation with all samples for each 100-grain-sized class within a measurement range of 0.02–2000 μm with a 0.1 Φ interval. The standard deviations evidenced the sensitive degree of each grain-size component to the distance variation along the dust conveying direction. Here, we used the grain-size classes vs. the standard deviation method to identify the grain-size intervals with the most variability along a depositional sequence. We derived the percentage contents of samples for each grain-size level (generally divided into the 100-grain grade) from grain-size data. Additionally, we calculated the standard deviation from the grain-size data. We calculated the grain-size classes vs. standard deviation figures by taking the grain size as the *X*-axis and the standard deviation as the *Y*-axis, from which sensitive grain-size components could be clearly obtained.

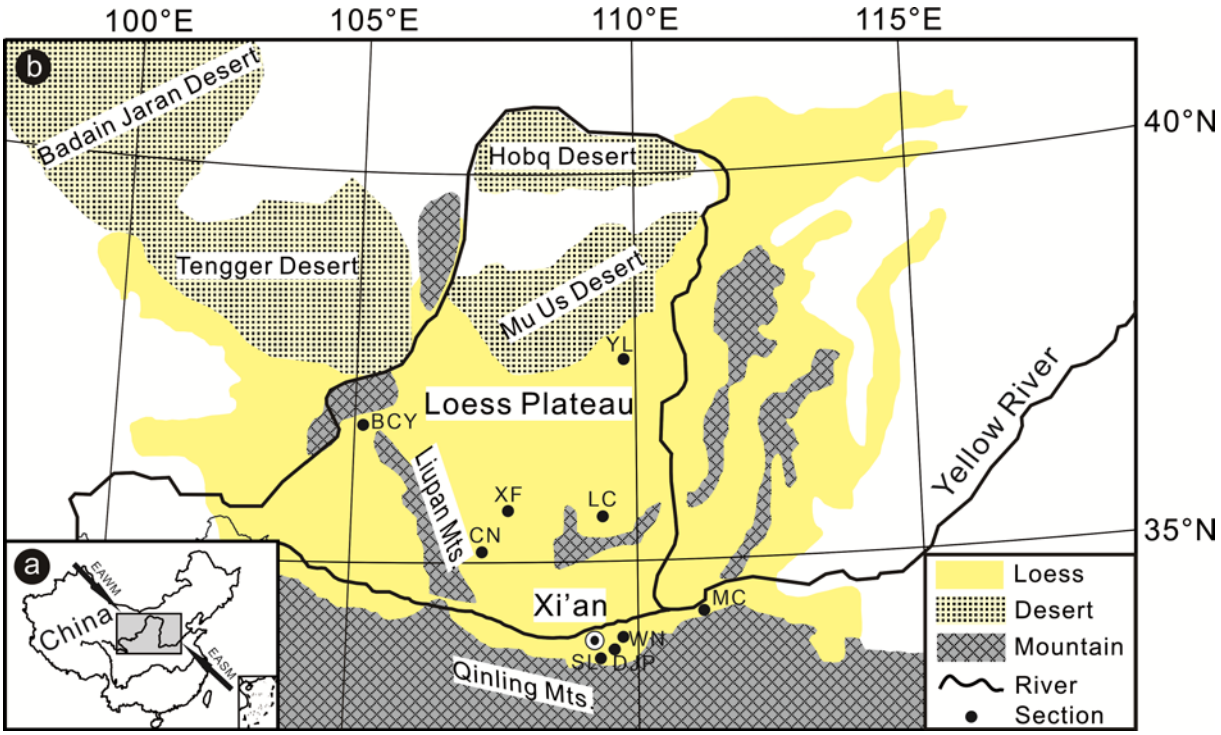

Figure 1. Map showing location of loess sections (black spot) (**a**) on Chinese Loess Plateau (**b**). YL: Yulin; BCY: Baicaoyuan; XF: Xifeng; LC: Luochuan; CN: Chaona; MC: Mianchi; WN: Weinan; DJP: Duanjiapo; SL: Shaoling; EASM: East Asian summer monsoon; EAWM: East Asian winter monsoon.

3. Results

According to the grain-size records of the nine loess sections, the grain-size class vs. standard deviation values are displayed in Figure 2.

Figure 2 shows that two or three typical peaks are observed in the grain-size classes vs. standard deviation curves of nine sections. The grain-size variations in the aeolian sediments are controlled by many factors. The Yulin section shows two standard deviation peaks at 39.9 μm and 141.6 μm, with size-range boundaries of 71.0 μm (Figure 2a). However, the Baicaoyuan section also has the three standard deviation peaks at 0.4 μm, 16.0 μm, and 69.2 μm corresponding to size ranges which are <0.8 μm, 0.8–31.7 μm, and >31.7 μm (Figure 2b). The three standard deviation peaks appear in the Xifeng section as 0.6 μm, 11.9 μm, and 56.9 μm, corresponding to size ranges of <0.8 μm, 0.8–26.1 μm, and >26.1 μm, respectively (Figure 2c). The Luochuan section also has two standard deviation peaks at 14.2 μm and 56.4 μm, with size ranges of <28.3 μm and >28.3 μm, respectively (Figure 2d). For the Chaona section, there are three obvious peaks on the grain-size class vs. standard deviation curves, namely 3.9 μm, 14.1 μm, and 50.2 μm, which correspond to size ranges of <5.6 μm, 5.6–28.3 μm, and >28.3 μm, respectively (Figure 2e). The Mianchi section shows two standard deviation peaks at 39.9 μm and 87.5 μm, which have size-range boundaries of 56.4 μm (Figure 2f). The Weinan and Shaoling sections show two standard deviation peaks at 2.9 μm and 30.2 μm, and 12.6 μm and 35.6 μm, respectively, which have size-range boundaries of 6.6 μm and 17.8 μm, respectively (Figure 2g,i). The Duanjiapo section has many peaks on the grain-size class vs. standard deviation curves, with the two main peaks at 10.8 μm and 46.8 μm, which have size ranges of <21.4 μm and >21.4 μm, respectively (Figure 2h).

We obtained the fine and coarse sensitive grain-size components data by performing the Mann–Whitney *U* statistic. The Mann–Whitney *U* statistic process is as follows.

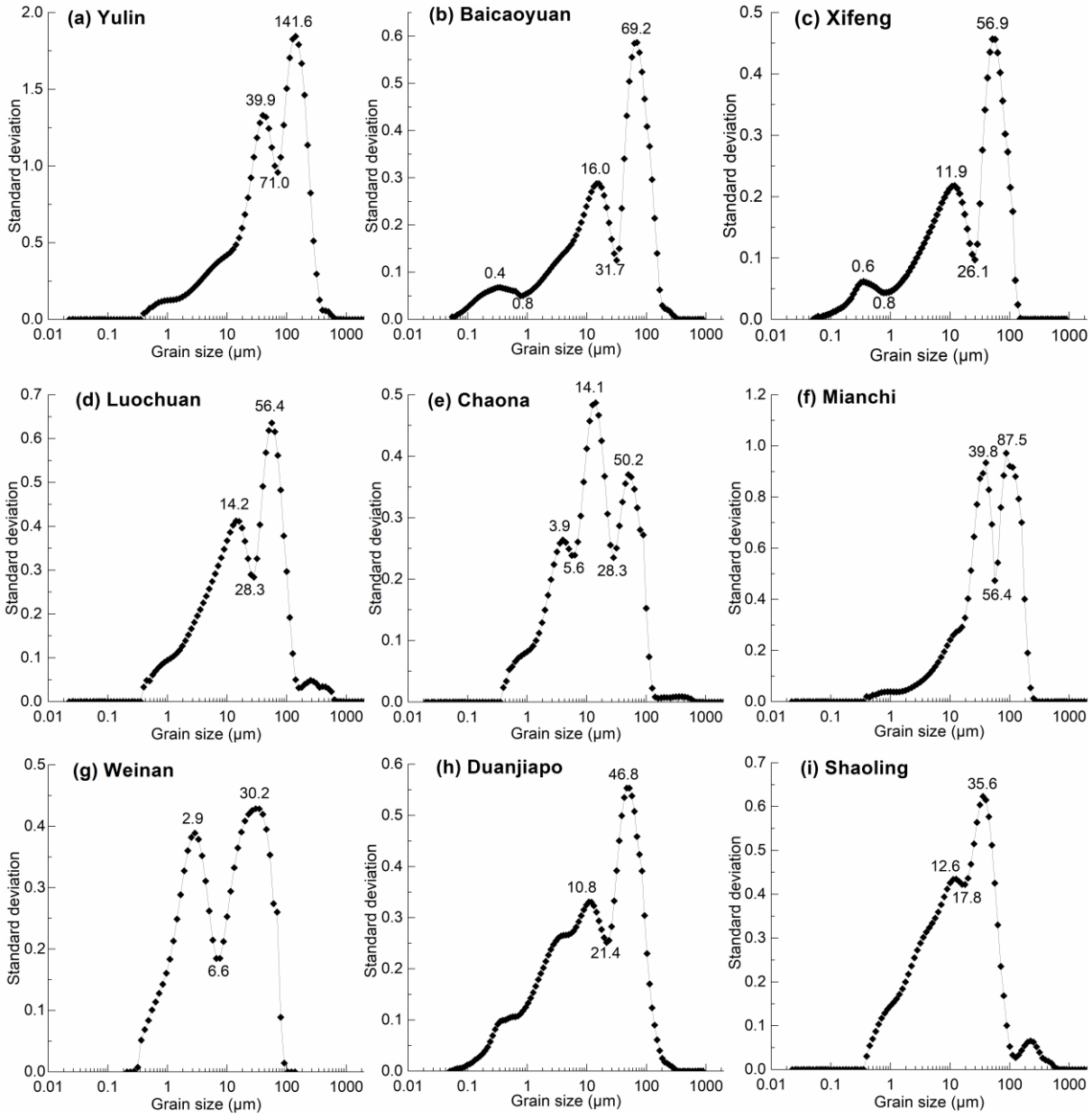

Figure 2. Grain-size classes vs. standard deviation curves of nine last glacial loess sections (**a**–**i**) on Chinese Loess Plateau.

The computation of the Mann–Whitney *U* statistic begins by arbitrarily designating two samples as fine- and coarse-size groups. The data from the two groups are combined into one group (Table 2), with each data value retaining a group identifier of its original group. The pooled values are then ranked from 1 to n, with the smallest value being assigned a rank of 1. The fine and coarse grain sizes are designated as Group 1 and 2, respectively (Table 3). n_1 is the amount of Group 1, while n_2 is the amount of Group 2 (both are 9). We computed and designated the sum of the ranks of the values from Group 1 and 2 as W_1 and W_2, respectively. According to Table 2, W_1 is 49 and W_2 is 122.

We hypothesized that there were no differences between the fine and coarse grain-size components except for their average values. We tested that H_0 had no difference the between fine and coarse grain size, whereas we tested that H_1 had a difference between the fine and coarse grain size.

Table 2. Ranks of fine and coarse grain size from nine loess sections.

Ranks	Grain Size	Ranks	Grain Size
1	2.90	10	39.80
2	10.80	11	39.90
3	11.90	12	46.80
4	12.60	13	50.20
5	14.10	14	56.40
6	14.20	15	56.90
7	16.00	16	69.20
8	30.20	17	87.50
9	35.60	18	141.60

Table 3. Groups of fine and coarse grain size from nine loess sections.

Group 1		Group 2	
Grain Size	**Ranks**	**Grain Size**	**Ranks**
39.90	11	141.80	18
16.00	7	69.20	16
11.90	3	56.90	15
14.20	6	56.40	14
14.10	5	50.20	13
39.80	10	87.50	17
2.90	1	30.20	8
10.80	2	46.80	12
12.60	4	35.60	9

The U_1 and U_2 values are calculated as follows

$$U_1 = n_1 n_2 + \frac{n_1(n_1+1)}{2} - W_1 \quad (1)$$

$$U_2 = n_1 n_2 + \frac{n_2(n_2+1)}{2} - W_2 \quad (2)$$

where the values n and W have been obtained, and we calculated the Mann–Whitney U statistic statistics, in which U_1 and U_2 are 77 and 4, respectively. The U_α (α = 0.05) can be obtained from the U statistic schedule, which is 17 in this study. Because of $U_2 < U_\alpha$, the test rejects H_0 and accepts H_1. Our results show that the fine and coarse components have significant differences. The grain-size class vs. standard deviation curves of our selected loess sections display the coarse and fine sensitive grain-size components. The fine and coarse components presented the CLP's spatial particle aggregation.

4. Discussion

4.1. Spatial Variations in Sensitive Grain-Size Components of Last Glacial Loess on CLP

The grain size of aeolian deposits is mainly affected by the source area, wind intensity, and weathering [10,17,29,38,56]. The loess deposits in the northern and northwestern regions have been relatively greater affected by the source area, and the weathering degree and pedogenesis have influenced and changed the particle-size distribution of the southeast loess [1,2,7,10,62]. According to the curves of the grain-size class vs. standard deviation (Figure 2), apart from the standard deviations of coarse and fine sensitive components in the Weinan and Mianchi sections being comparable, the sensitive coarse grain-size compositions of the Luochuan, Yulin, Xifeng, Shaoling, and Baicaoyuan sections have a higher standard deviation than the fine grain-size components. This indicated that the content of coarse particles can better reflect the sedimentary environment changes. The sensitive grain-size components of the Yulin, Baicaoyuan, Xifeng, and Luochuan sections were coarser, being more influenced by the distance from material resources, whereas the

Weinan, Shaoling Duanjiapo, and Chaona sections were finer as they were more influenced by the weathering degree and pedogenesis. The sensitive grain-size components of the Mianchi section were also coarser, which may be affected by local circulation and the nearby Yellow River terrace.

Because the size ranges define the limits of classes, the grain-size component of the maximum peak belongs to the sand component, which with the intermediate peak belongs to the silt component [10,28,62], while the minimum peak mainly belongs to the silt component. Figure 2 shows that the sand component of the nine loess sections has the highest standard deviation value. Thus, the sand component displays a decreasing trend from northwest to southeast on the CLP. The silt component of the nine loess sections also decreases gradually. The clay and fine silt components from Xifeng, Luochuan, Shaoling, Weinan, Baicaoyuan, and Duanjiapo are mainly delivered in suspension transport by the high-level air current far away from the source area. Therefore, the fine grain-size component is not a suitable proxy indicator for the loess from the CLP. The standard deviation went to zero in the grain-size data of some loess sections, which mainly appeared in the superfine and coarse powder in the grain size-standard deviation curves (Figure 2). However, the superfine grain-size intervals were very small and divided into many more grain-size classes, which was one of the main reasons for the standard deviation to zero.

According to the two sensitive components, the coarse component in most loess sections has the largest standard deviation (Figure 2), with the highest degree of sensitivity for paleoclimatic changes, suggesting that this component is the most sensitive to the variation in source-to-sink distance. Thus, the coarse particle component is the most suitable proxy indicator of the last glacial loess.

4.2. The EAWM Implicated by Coarse Sensitive Grain-Size Component

Grain size is commonly used as a proxy for EAWM intensity, with higher values in glacial loess and lower values in interglacial paleosols [2,3,10,26,40,42]. Furthermore, magnetic susceptibility (MS) is also commonly used for EASM intensity, with the loess and paleosols layers showing lower and higher MS values, respectively [3,72–75]. Therefore, in our study, we used mean grain size (MGS) and low-frequency MS. The coarse grain-size component and MGS from the selected loess sections have a decreasing trend from northwest to southeast on the CLP (Figure 3), indicating the EAWM's gradually weakening trend.

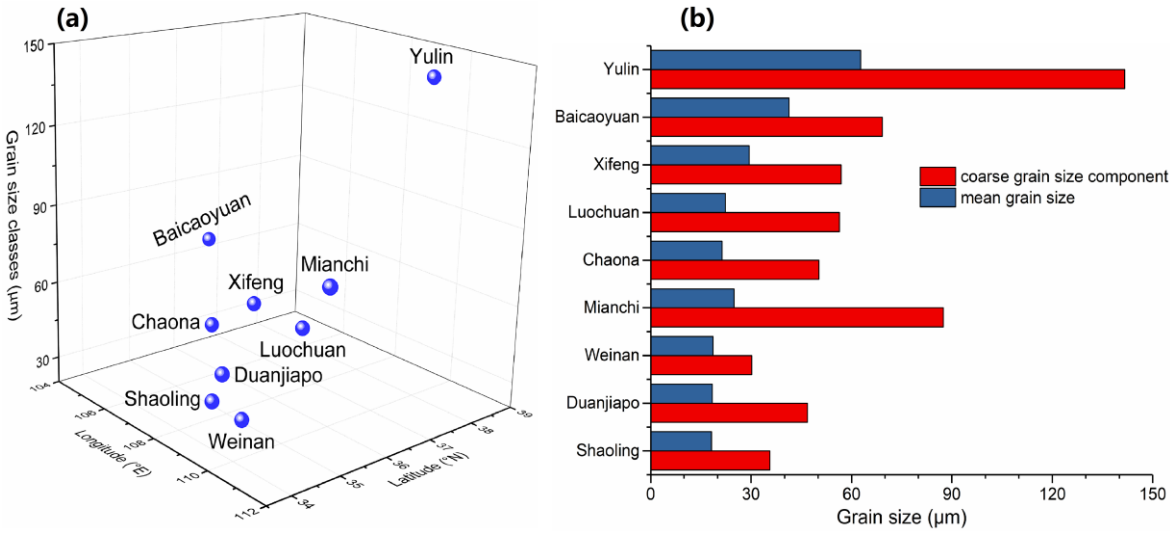

Figure 3. Variations in coarse particle size by scatter plot (**a**) and bar graph (**b**) from nine last glacial loess sections.

To further explore the variations in the EAWM, we selected MGS and MS to study the spatial changes (Figures 4 and 5). The results showed that the MGS decreased from

the northwest to the southeast on the CLP (Figure 5a), whereas the MS increased from the northwest to the southeast (Figure 5b). This indicated that the EAWM intensity gradually weakened following the variations in MGS. At the same time, the EASM intensity gradually enhanced following the variations in MS. The decreased coarse grain size and increased fine grain size corresponded with the distance of the EAWM from the Asian high-pressure center and dust source. In addition, the fine grain-size components that were linked to pedogenesis were affected by the EASM's rainfall.

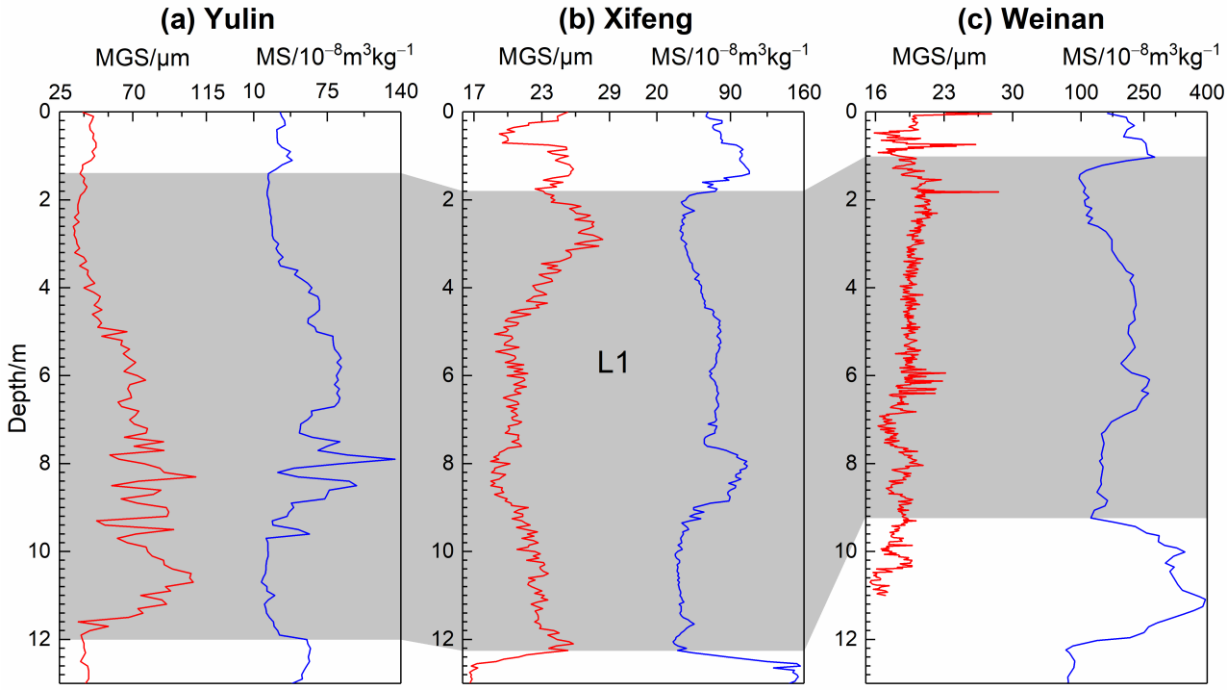

Figure 4. Variations in mean grain size (MGS; red) and magnetic susceptibility (MS; blue) of Yulin (**a**), Xifeng (**b**), and Weinan (**c**) loess sections in last glacial period. The gray area indicates last glacial loess.

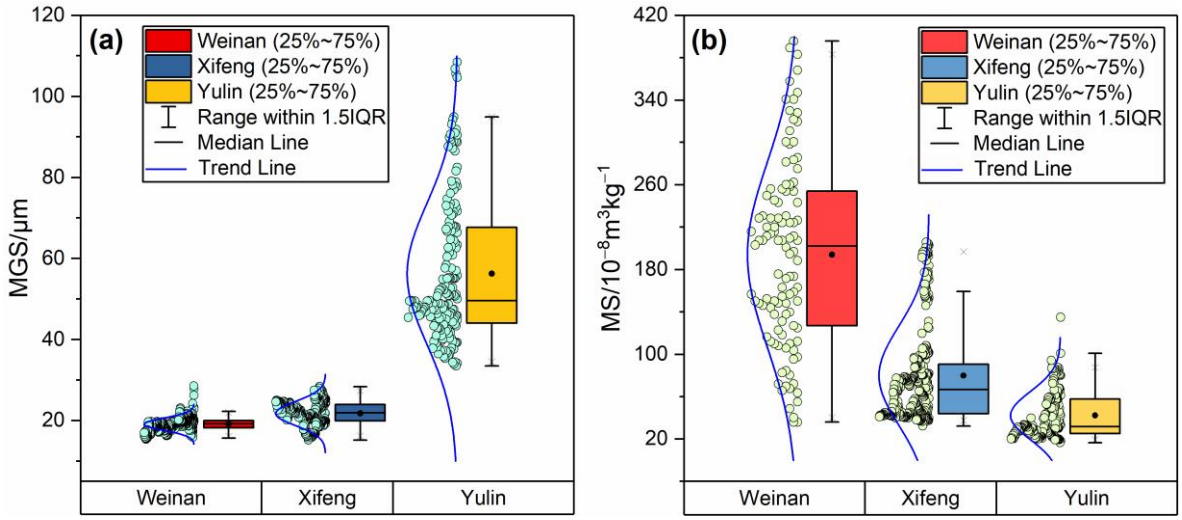

Figure 5. Boxplots of mean grain size (MGS) (**a**) and magnetic susceptibility (MS) (**b**) (with percentiles 2.5, 25, 50, 75, 97.5%) from Yulin, Xifeng, and Weinan loess sections.

Above all, the spatial variations in the coarse grain-size component of the last glacial loess can better reflect the evolution of EAWM on the CLP. We interpret the decreasing trend in grain size and coarse sensitive size component from northwest to southeast as

gradually weakening from the EAWM. The sedimental grain size appears to be arranged from large to small in the northwest and southeast, respectively, which indicates that the sensitive coarse grain-size component is a sensitive proxy for the EAWM's variability.

5. Conclusions

Using the grain-size class vs. standard deviation method, we extracted the environmentally sensitive grain-size components based on the grain size of the nine last glacial loess sections. Among the sensitive grain-size components, the coarse particle size in most loess sections has the highest standard deviation. It also has the most degree of sensitivity, suggesting that the coarse-particle component is the most sensitive to the variations in source-to-sink distance. The coarse grain-size components also have a decreasing trend from northwest to southeast on the CLP. Comparisons between the coarse grain-size component and mean grain size reveal that the coarse grain-size components decrease along with the weakening of the EAWM from the northwest to the southeast on the CLP, which can be regarded as a suitable proxy indicator of grain size and the EAWM on the CLP. More evidence regarding grain size is needed in the future to reflect the evolution process of the EAWM and atmospheric circulation.

Author Contributions: Funding acquisition, Q.W. and Y.S.; writing—original draft preparation, Q.W.; writing—review and editing, Y.S. and L.D.; visualization, J.L. All authors have read and agreed to the published version of the manuscript.

Funding: This research was funded by the Strategic Priority Research Program of the Chinese Academy of Sciences (XDB26000000), the National Natural Science Foundation of China (Grant No. 41807287), and the Shandong Provincial Natural Science Foundation (No. ZR2017BD017).

Institutional Review Board Statement: Not applicable.

Informed Consent Statement: Not applicable.

Data Availability Statement: The datasets of this study are available from https://figshare.com/s/4320fb0983f7a5a47f91, accessed on 2 February 2023.

Acknowledgments: Many thanks to Junchao Dong for their field and lab assistance, and Xiaodong Miao for discussion. We are grateful for the two reviewers' critical comments and suggestions.

Conflicts of Interest: The authors declare no conflict of interest.

References

1. An, Z.; Liu, T.; Lu, Y.; Porter, S.C.; Kukla, G.; Wu, X.; Hua, Y. The long-term paleomonsoon variation recorded by the loess-paleosol sequence in central China. *Quat. Int.* **1990**, *7–8*, 91–95.
2. An, Z.; Kukla, G.; Porter, S.C.; Xiao, J. Late Quaternary dust flow on the Chinese Loess Plateau. *Catena* **1991**, *18*, 125–132. [CrossRef]
3. An, Z. *Late Cenozoic Climate Change in Asia: Loess, Monsoon and Monsoon-Arid Environment Evolution*; Developments in Paleoenvironmental Research; Springer: Berlin/Heidelberg, Germany, 2014.
4. Liu, T.S. *Loess and the Environment*; Science Press: Beijing, China, 1985.
5. Kukla, G.; An, Z. Loess stratigraphy in Central China. *Palaeogeogr. Palaeoclimatol. Palaeoecol.* **1989**, *72*, 203–225. [CrossRef]
6. Lu, H.; Sun, D. Pathways of dust input to the Chinese Loess Plateau during the last glacial and interglacial periods. *Catena* **2000**, *40*, 251–261. [CrossRef]
7. Maher, B.A. Palaeoclimatic records of the loess/palaeosol sequences of the Chinese Loess Plateau. *Quat. Sci. Rev.* **2016**, *154*, 23–84. [CrossRef]
8. Muhs, D.R.; Bettis, A.E. Quaternary loess-Paleosol sequences as examples of climate-driven sedimentary extremes. *Geol. Soc. Am. Spec. Pap.* **2003**, *370*, 53–74.
9. Porter, S.C. Chinese loess record of monsoon climate during the last glacial–interglacial cycle. *Earth-Sci. Rev.* **2001**, *54*, 115–128. [CrossRef]
10. Sun, Y.; Chen, J.; Clemens, S.C.; Liu, Q.; Ji, J.; Tada, R. East Asian monsoon variability over the last seven glacial cycles recorded by a loess sequence from the northwestern Chinese Loess Plateau. *Geochem. Geophys. Geosyst.* **2006**, *7*. [CrossRef]
11. Xu, X.; Qiang, X.; Hu, S.; Zhao, H.; Fu, C.; Zhao, Q. Records of the Mid-Brunhes Event in Chinese loess-paleosol sequences. *Palaeogeogr. Palaeoclimatol. Palaeoecol.* **2020**, *543*, 109596. [CrossRef]

12. Zhang, X.; An, Z.; Chen, T.; Zhang, G.Y.; Arimoto, R.; Ray, B.J. Late Quaternary records of the atmospheric input of eolian dust to the center of the Chinese Loess Plateau. *Quat. Res.* **1994**, *41*, 35–43. [CrossRef]
13. Zhao, H.; Qiang, X.; Xu, X.; Sun, Y. Iron oxide characteristics of the Chinese loess-red clay sequences and their implications for the evolution of the East Asian summer monsoon since the Late Oligocene. *Palaeogeogr. Palaeoclimatol. Palaeoecol.* **2020**, *543*, 109604. [CrossRef]
14. Sun, Y.; Clemens, S.C.; Guo, F.; Liu, X.; Wang, Y.; Yan, Y.; Liang, L. High-sedimentation-rate loess records: A new window into understanding orbital- and millennial-scale monsoon variability. *Earth-Sci. Rev.* **2021**, *220*, 103731. [CrossRef]
15. Liu, T.; Ding, Z. Chinese loess and the paleomonsoon. *Annu. Rev. Earth Planet. Sci.* **1998**, *26*, 111–145. [CrossRef]
16. Újvári, G.; Kok, J.F.; Varga, G.; Kovács, J. The physics of windblown loess: Implications for grain size proxy interpretations in Quaternary paleoclimate studies. *Earth-Sci. Rev.* **2016**, *154*, 247–278. [CrossRef]
17. Chen, G.; Zheng, H.; Li, J.; Xie, X.; Mei, X. Dynamic control on grain-size distribution of terrigenous sediments in the western South China Sea: Implication for East Asian monsoon evolution. *Chin. Sci. Bull.* **2008**, *53*, 1533–1543. [CrossRef]
18. Hu, P.; Liu, Q.; Torrent, J.; Barrón, V.; Jin, C. Characterizing and quantifying iron oxides in Chinese loess/paleosols: Implications for pedogenesis. *Earth Planet. Sci. Lett.* **2013**, *369–370*, 271–283. [CrossRef]
19. Hu, P.; Liu, Q.; Heslop, D.; Roberts, A.P.; Jin, C. Soil moisture balance and magnetic enhancement in loess–paleosol sequences from the Tibetan Plateau and Chinese Loess Plateau. *Earth Planet. Sci. Lett.* **2015**, *409*, 120–132. [CrossRef]
20. Jia, J.; Wang, B.; Lu, C.; Wang, Y.; Zhu, L.; Xia, D. New insights into the magnetic characteristics of high mountain loess in Central Asia and its paleoclimatic implications. *Quat. Int.* **2019**, *502*, 71–77. [CrossRef]
21. Nie, J.; King, J.W.; Fang, X. Enhancement mechanisms of magnetic susceptibility in the Chinese red-clay sequence. *Geophys. Res. Lett.* **2007**, *34*. [CrossRef]
22. Nie, J.; Song, Y.; King, J.W.; Egli, R. Consistent grain size distribution of pedogenic maghemite of surface soils and Miocene loessic soils on the Chinese Loess Plateau. *J. Quat. Sci.* **2010**, *25*, 261–266. [CrossRef]
23. Song, Y.; Fang, X.; King, J.W.; Li, J.; Naoto, I.; An, Z. Magnetic parameter variations in the Chaona loess/paleosol sequences in the central Chinese Loess Plateau, and their significance for the middle Pleistocene climate transition. *Quat. Res.* **2014**, *81*, 433–444. [CrossRef]
24. Sun, D.; Su, R.; Bloemendal, J.; Lu, H. Grain-size and accumulation rate records from Late Cenozoic aeolian sequences in northern China: Implications for variations in the East Asian winter monsoon and westerly atmospheric circulation. *Palaeogeogr. Palaeoclimatol. Palaeoecol.* **2008**, *264*, 39–53. [CrossRef]
25. Sun, Y.; Wang, X.; Liu, Q.; Clemens, S.C. Impacts of post-depositional processes on rapid monsoon signals recorded by the last glacial loess deposits of northern China. *Earth Planet. Sci. Lett.* **2010**, *289*, 171–179. [CrossRef]
26. Zan, J.; Li, X.; Fang, X.; Zhang, W.; Yan, M.; Mao, Z. Grain-size analysis of Upper Pliocene red clay deposits from Linxia Basin: Implications for Asian monsoon evolution on the NE margin of the Tibetan Plateau. *Palaeogeogr. Palaeoclimatol. Palaeoecol.* **2018**, *511*, 597–605. [CrossRef]
27. Zeng, L.; Lu, H.; Yi, S.; Stevens, T.; Xu, Z.; Zhuo, H.; Yu, K.; Zhang, H. Long-term Pleistocene aridification and possible linkage to high-latitude forcing: New evidence from grain size and magnetic susceptibility proxies from loess-paleosol record in northeastern China. *Catena* **2017**, *154*, 21–32. [CrossRef]
28. Doeglas, D.J. Grain-size indices, classification and environment. *Sedimentology* **1968**, *10*, 83–100. [CrossRef]
29. Chen, F.; Feng, Z.; Zhang, J. Loess particle size data indicative of stable winter monsoons during the last interglacial in the western part of the Chinese Loess Plateau. *Catena* **2000**, *39*, 233–244. [CrossRef]
30. Li, X.; Zan, J.; Yang, R.; Fang, X.; Yang, S. Grain-size-dependent geochemical characteristics of Middle and Upper Pleistocene loess sequences from the Junggar Basin: Implications for the provenance of Chinese eolian deposits. *Palaeogeogr. Palaeoclimatol. Palaeoecol.* **2020**, *538*, 109458. [CrossRef]
31. Lin, Y.; Mu, G.; Xu, L.; Zhao, X. The origin of bimodal grain-size distribution for aeolian deposits. *Aeolian Res.* **2016**, *20*, 80–88. [CrossRef]
32. Wang, Y.; Lu, H. Stepwise coupling between Chinese loess deposition and global temperature since the early Pleistocene tested by a multiple-state model. *Quat. Int.* **2022**, *620*, 4–12. [CrossRef]
33. Zhou, X.; Yang, W.; Xiang, R.; Wang, Y.; Sun, L. Re-examining the potential of using sensitive grain size of coastal muddy sediments as proxy of winter monsoon strength. *Quatern. Int.* **2014**, *333*, 173–178. [CrossRef]
34. Liu, X.; Sun, Y.; Vandenberghe, J.; Li, Y.; An, Z. Palaeoenvironmental implication of grain-size compositions of terrace deposits on the western Chinese Loess Plateau. *Aeolian Res.* **2018**, *32*, 202–209. [CrossRef]
35. Liu, X.; Vandenberghe, J.; An, Z.; Li, Y.; Jin, Z.; Dong, J.; Sun, Y. Grain size of Lake Qinghai sediments: Implications for riverine input and Holocene monsoon variability. *Palaeogeogr. Palaeoclimatol. Palaeoecol.* **2016**, *449*, 41–51. [CrossRef]
36. Lu, H.; An, Z. Palaeoclimatic significance of grain size of loess–palaeosol sequence of Central China. *Sci. China Series D-Earth Sci.* **1998**, *41*, 626–631. [CrossRef]
37. Paterson, G.A.; Heslop, D. New methods for unmixing sediment grain size data. *Geochem. Geophys. Geosyst.* **2015**, *16*, 4494–4506. [CrossRef]
38. Sun, D.; Bloemendal, J.; Rea, D.K.; Vandenberghe, J.; Jiang, F.; An, Z.; Su, R. Grain-size distribution function of polymodal sediments in hydraulic and aeolian environments, and numerical partitioning of the sedimentary components. *Sed. Geol.* **2002**, *152*, 263–277. [CrossRef]

39. Tian, S.; Sun, J.; Gong, Z. Loess deposits in Beijing and their paleoclimatic implications during the last interglacial-glacial cycle. *Quat. Sci. Rev.* **2017**, *177*, 78–87. [CrossRef]
40. Vandenberghe, J. Grain size of fine-grained windblown sediment: A powerful proxy for process identification. *Earth-Sci. Rev.* **2013**, *121*, 18–30. [CrossRef]
41. Vandenberghe, J.; Sun, Y.; Wang, X.; Abels, H.A.; Liu, X. Grain-size characterization of reworked fine-grained aeolian deposits. *Earth-Sci. Rev.* **2018**, *177*, 43–52. [CrossRef]
42. Xiao, J.; Porter, S.C.; An, Z.; Kumai, H.; Yoshikawa, S. Grain Size of Quartz as an Indicator of Winter Monsoon Strength on the Loess Plateau of Central China during the Last 130,000 Yr. *Quat. Res.* **1995**, *43*, 22–29. [CrossRef]
43. Xiao, J.; Chang, Z.; Fan, H.; Zhou, L.; Xhai, D.; Wen, R.; Qin, X. The link between grain-size components and depositional processes in a modern clastic lake. *Sedimentology* **2012**, *59*, 1050–1062. [CrossRef]
44. Chen, J.; Yang, T.; Qiang, M.; Matishov, G.G.; Velichko, A.A.; Zeng, B.; Xu, M.; Shi, P. Interpretation of sedimentary subpopulations extracted from grain size distributions in loess deposits at the Sea of Azov, Russia. *Aeolian Res.* **2020**, *45*, 100597. [CrossRef]
45. Hou, K.; Qian, H.; Zhang, Y.; Qu, W.; Ren, W.; Wang, H. Relationship between fractal characteristics of grain-size and physical properties: Insights from a typical loess profile of the loess Plateau. *Catena* **2021**, *207*, 105653. [CrossRef]
46. Sprafke, T.; Schulte, P.; Meyer-Heintze, S.; Händel, M.; Einwögerer, T.; Simon, U.; Peticzka, R.; Schäfer, C.; Lehmkuhl, F.; Terhorst, B. Paleoenvironments from robust loess stratigraphy using high-resolution color and grain-size data of the last glacial Krems-Wachtberg record (NE Austria). *Quat. Sci. Rev.* **2020**, *248*, 106602. [CrossRef]
47. Jia, Y.; Zhang, Y.; Huang, C.; Wang, N.; Qiu, H.; Wang, H.; Xiao, Q.; Chen, D.; Lin, X.; Zhu, Y.; et al. Late Pleistocene-Holocene aeolian loess-paleosol sections in the Yellow River source area on the northeast Tibetan Plateau: Chronostratigraphy, sediment provenance, and implications for paleoclimate reconstruction. *Catena* **2022**, *208*, 105777. [CrossRef]
48. Wei, G.; Zhang, C.; Li, Q.; Wang, R.; Wang, H.; Zhang, Y.; Yuan, Y.; Li, Y. Grain-size composition of the surface sediments in Chinese deserts and the associated dust emission. *Catena.* **2022**, *219*, 106615. [CrossRef]
49. Nugteren, G.; Vandenberghe, J. Spatial climatic variability on the Central Loess Plateau (China) as recorded by grain size for the last 250 kyr. *Glob. Planet. Chang.* **2004**, *41*, 185–206. [CrossRef]
50. Sun, Y.; Lu, H.; An, Z. Grain size of loess, palaeosol and Red Clay deposits on the Chinese Loess Plateau: Significance for understanding pedogenic alteration and palaeomonsoon evolution. *Palaeogeogr. Palaeoclimatol. Palaeoecol.* **2006**, *241*, 129–138. [CrossRef]
51. Wen, L.; Lu, H.; Qiang, X. Changes in grain-size and sedimentation rate of the Neogene Red Clay deposits along the Chinese Loess Plateau and implications for the palaeowind system. *Sci. China Ser. D* **2005**, *48*, 1452–1462. [CrossRef]
52. Prins, M.A.; Vriend, M.; Nugteren, G.; Vandenberghe, J.; Lu, H.Y.; Zheng, H.B.; Weltje, G.J. Late Quaternary aeolian dust input variability on the Chinese Loess Plateau: Inferences from unmixing of loess grain-size records. *Quat. Sci. Rev.* **2007**, *435*, 254–264. [CrossRef]
53. Schulte, P.; Lehmkuhl, F. The difference of two laser diffraction patterns as an indicator for post-depositional grain size reduction in loess-paleosol sequences. *Palaeogeogr. Palaeoclimatol. Palaeoecol.* **2018**, *509*, 126–136. [CrossRef]
54. Sun, Y.; Gao, S.; Li, J. Preliminary analysis of grain-size populations with environmentally sensitive terrigenous components in marginal sea setting. *Chin. Sci. Bull.* **2003**, *48*, 184–187. [CrossRef]
55. Vriend, M.; Prins, M.A.; Buylaert, J.P.; Vandenberghe, J.; Lu, H. Contrasting dust supply patterns across the north-western Chinese Loess Plateau during the last glacial-interglacial cycle. *Quat. Int.* **2011**, *240*, 167–180. [CrossRef]
56. Ding, Z.; Yu, Z.; Yang, S.; Sun, J.; Xiong, S.; Liu, T. Coeval changes in grain size and sedimentation rate of eolian loess, the Chinese Loess Plateau. *Geophys. Res. Lett.* **2001**, *28*, 2097–2100. [CrossRef]
57. Nottebaum, V.; Stauch, G.; Hartmann, K.; Zhang, J.; Lehmkuhl, F. Unmixed loess grain size populations along the northern Qilian Shan (China): Relationships between geomorphologic, sedimentologic and climatic controls. *Quat. Int.* **2015**, *372*, 151–166. [CrossRef]
58. Vandenberghe, J.; An, Z.; Nugteren, G.; Lu, H.; Van Huissteden, J. New absolute time scale for the Quaternary climate in the Chinese loess region by grain-size analysis. *Geology* **1997**, *25*, 35–38. [CrossRef]
59. Boulay, S.; Colin, C.; Trentesaux, A.; Pluquet, F.; Bertaux, J.; Blamart, D.; Buehring, C.; Wang, P. Mineralogy and sedimentology of Pleistocene sediment in the South China Sea (ODP Site 1144). Proceedings of the Ocean Drilling Program. *Sci. Results* **2003**, *184*, 1–21.
60. Xu, S.; Ding, X.; Yu, L.; Ni, Z. Palaeoclimatic implications of aeolian sediments on the Miaodao Islands, Bohai Sea, East China, based on OSL dating and proxies. *Aeolian Res.* **2015**, *19*, 259–266. [CrossRef]
61. Peng, Y.; Xiao, J.; Nakamura, T.; Liu, B.; Inouchi, Y. Holocene East Asian monsoonal precipitation pattern revealed by grain-size distribution of core sediments of Daihai Lake in Inner Mongolia of north-central China. *Earth Planet. Sci. Lett.* **2005**, *233*, 467–479. [CrossRef]
62. Guan, Q.; Zhang, J.; Wang, L.; Pan, B.; Gui, H.; Zhang, C. Discussion of the relationship between dustfall grain size and the desert border, taking the southern border of the Tengger Desert and the southern dust deposit area as an example. *Palaeogeogr. Palaeoclimatol. Palaeoecol.* **2013**, *386*, 1–7. [CrossRef]
63. Huang, J.; Li, A.C.; Wan, S.M. Sensitive grain-size records of Holocene East Asian summer monsoon in sediments of northern South China Sea slope. *Quat. Res.* **2017**, *75*, 734–744. [CrossRef]

64. Xiang, R.; Yang, Z.; Yoshiki, S.; Guo, Z.; Fan, D.; Li, Y.; Xiao, S.; Shi, X.; Chen, M. East Asia Winter Monsoon changes inferred from environmentally sensitive grain-size component records during the last 2300 years in mud area southwest off Cheju Island, ECS. *Sci. China, Ser. D* **2006**, *49*, 604–614. [CrossRef]
65. Xiao, S.; Li, A.; Liu, J.P.; Chen, M.; Xie, Q.; Jiang, F.; Li, T.; Xiang, R.; Chen, Z. Coherence between solar activity and the East Asian winter monsoon variability in the past 8000 years from Yangtze River-derived mud in the East China Sea. *Palaeogeogr. Palaeoclimatol. Palaeoecol.* **2006**, *237*, 293–304. [CrossRef]
66. Fan, D.; Qi, H.; Sun, X.; Liu, Y.; Yang, Z. Annual lamination and its sedimentary implications in the Yangtze River delta inferred from High-resolution biogenic silica and sensitive grain-size records. *Cont. Shelf Res.* **2011**, *31*, 129–137. [CrossRef]
67. Meyer, I.; Daele, M.V.; Tanghe, N.; Batist, M.D.; Verschuren, D. Reconstructing East African monsoon variability from grain-size distributions: End-member modeling and source attribution of diatom-rich sediments from Lake Chala. *Quat. Sci. Rev.* **2020**, *247*, 106574. [CrossRef]
68. De Mahiques, M.M.; YGoya, S.C.; Da Silva, M.C.; De Oliveira, R.A.U.; Mi Kim, B.S.; De Lima Ferreira, P.A.; Lopes Figueira, R.C.; Bícegoa, M.C. Grain-size end-members and environmentally sensitive grain-size components: A comparative study in the mud shelf depocenters off southern Brazil. *Int. J. Sediment Res.* **2021**, *36*, 317–327. [CrossRef]
69. Kong, F.; Xu, S.; Han, M.; Chen, H.; Miao, X.; Kong, X.; Jia, G. Application of grain size endmember analysis in the study of dust accumulation processes: A case study of loess in Shandong Province, East China. *Sediment. Geol.* **2021**, *416*, 105868. [CrossRef]
70. Lai, H.C.; Zhang, J.F.; Li, Y.Y.; Zhou, L.P. Origin and provenance of Red Clay in north Hunan Province, China: Inferred from grain-size analysis and end-member modelling. *Aeolian Res.* **2021**, *51*, 100714. [CrossRef]
71. Lu, H.; An, Z. Pretreated methods on loess-palaeosol samples granulometry. *Chin. Sci. Bull.* **1998**, *43*, 237–240. [CrossRef]
72. An, Z.; Kukla, G.J.; Porter, S.C.; Xiao, J. Magnetic susceptibility evidence of monsoon variation on the Loess Plateau of Central China during the last 130,000 years. *Quat. Res.* **1991**, *36*, 29–36. [CrossRef]
73. An, Z.; Porter, S.C. Millennial-scale climatic oscillations during the last interglaciation in central China. *Geology* **1997**, *25*, 603–606. [CrossRef]
74. Fang, X.; Ono, Y.; Fukusawa, H.; Pan, B.; Li, J.; Guan, D.; Oi, K.; Tsukamoto, S.; Torii, M.; Mishima, T. Asian summer monsoon instability during the past 60,000 years: Magnetic susceptibility and pedogenic evidence from the western Chinese Loess Plateau. Earth Planet. *Sci. Lett.* **1999**, *168*, 219–232.
75. Kong, X.; Zhou, W.; Back, J.; Xian, F.; Qiang, X.; Ao, H.; Wu, Z.; An, Z. Loess magnetic susceptibility flux: A new proxy of East Asian monsoon precipitation. *J. Asian Earth Sci.* **2020**, *201*, 104489. [CrossRef]